

Micropore-Rich Yolk-Shell N-doped Carbon Spheres: An Ideal Electrode Material for High-Energy Capacitive Energy Storage

Xinyuan Li,^[a] Zhenhui Liu,^[a] Congcong Cai,^[a] Qiang Yu,^[a] Wenting Jin,^[a] Ming Xu,^[a] Chang Yu,^[a] Shidong Li,^[a] Liang Zhou,^{*[a, b]} and Liqiang Mai^{*[a, b]}

Increasing the energy density of electrochemical double layer capacitors (EDLCs) can broaden their applications in energy storage but remains a formidable challenge. Herein, micropore-rich yolk-shell structured N-doped carbon spheres (YSNCs) were constructed by a one-pot surfactant-free self-assembly method in aqueous solution. The resultant YSNCs after activation possessed an ultrahigh surface area of 2536 m²g⁻¹,

among which 80% was contributed from micropores. When applied in EDLCs, the activated YSNCs demonstrated an unprecedentedly high capacitance (270 Fg⁻¹ at 1 Ag⁻¹) in 1-ethyl-3-methylimidazolium tetrafluoroborate ([EMIM][BF₄]) ionic liquid, affording an ultrahigh energy density (133 Whkg⁻¹ at 943 Wkg⁻¹). The present contribution provides insight into engineering porous carbons for capacitive energy storage.

Introduction

Electrochemical double layer capacitors (EDLCs) play an irreplaceable role in energy storage owing to their unique merits such as high power density, short charging time, and long service life.^[1] However, EDLCs generally possess quite limited energy density. Such a situation is originated from their distinct charge storage mechanisms: the EDLCs operate on ion adsorption/desorption at the electrode/electrolyte interface.^[2] To broaden the application in energy storage, the energy density bottleneck of EDLCs should be tackled, which puts forward strict requirements on electrode materials and matching electrolytes.

Porous carbons are the electrode material of choice for EDLCs owing to their high surface area, extraordinary electrical conductivity, tunable pore size, low cost, and natural abundance.^[3] Different types of porous carbons, such as microporous carbon,^[4] mesoporous carbon,^[5] graphene,^[6] carbon nanotubes,^[7] nanofibers,^[8] nanosheets,^[9] nanocages,^[10] and porous carbon microspheres,^[11] have been rationally designed for EDLCs. Among the various structures, porous carbon microspheres are especially attractive owing to their ability to minimize aggregation and

maximize the packing density in electrodes. Engineering the surface area, pore size, microstructure, crystallinity, and surface functionality of porous carbon microspheres holds the key to boost the capacitive performance. For example, Luo et al. designed porous carbon microspheres with high surface area and high graphitization degree by introducing activation agent and graphitization catalyst simultaneously.^[12] The resultant porous carbon microspheres demonstrated high capacitance and rate capability in aqueous electrolyte.

Yolk-shell carbon spheres (YSCSs), which are composed of a spherical/non-spherical carbon core encapsulated in a hollow carbon shell, represent a special type of porous carbon microspheres.^[13] Compared to hollow carbon spheres, the YSCSs possess higher bulk density and thus higher volumetric capacitance. Compared to solid porous carbon spheres, the YSCSs possess more porosity and thus higher gravimetric capacitance. Thus, the YSCSs offer a better trade-off between volumetric and gravimetric capacitance than the hollow carbon and solid porous carbon sphere counterparts. Qiao et al. developed a “silica-assisted” approach towards YSCSs and evaluated the capacitive performance.^[14] Liu et al. prepared a series of YSCSs^[15] employing either resin or dopamine as the carbon precursor and studied their capacitive performances in 1.0 M H₂SO₄. Recently, Liu et al. constructed asymmetric yolk-shell carbon microspheres through a heterogeneous contraction strategy,^[16] and the obtained material manifested a capacitance of 283 Fg⁻¹ in KOH. Without exception, the capacitive properties of YSCSs were studied in aqueous electrolytes. Although the YSCSs are able to achieve high capacitance in aqueous electrolytes, the narrow electrochemical window of aqueous electrolytes significantly limits the energy density of EDLCs. Replacing the aqueous electrolytes with organic electrolytes or ionic liquids (ILs) with wide electrochemical window would boost the energy density of EDLCs substantially.^[17] However, to the best of our knowledge, the capacitive performances of YSCSs in organic electrolytes or ILs have not been reported yet.

[a] X. Li, Dr. Z. Liu, C. Cai, Dr. Q. Yu, W. Jin, M. Xu, C. Yu, S. Li, Prof. L. Zhou, Prof. L. Mai
State Key Laboratory of Advanced Technology
for Materials Synthesis and Processing
Wuhan University of Technology
Luoshi Road 122, Wuhan,
430070 (P. R. China)
E-mail: liangzhou@whut.edu.cn
mlq518@whut.edu.cn

[b] Prof. L. Zhou, Prof. L. Mai
Foshan Xianhu Laboratory of the
Advanced Energy Science and
Technology Guangdong Laboratory
Xianhu Hydrogen Valley,
Foshan 528200 (P. R. China)

 Supporting information for this article is available on the WWW under <https://doi.org/10.1002/cssc.202100113>

Herein, we propose a one-pot surfactant-free self-assembly synthetic strategy in aqueous solution for the construction of yolk-shell N-doped carbon spheres (YSNCSs). The YSNCSs after activation possess a high surface area ($2536 \text{ m}^2 \text{ g}^{-1}$), abundant micropores, suitable pore size distribution, in-situ N doping, and excellent wettability for [EMIM][BF₄]. The above features endow the activated YSNCSs ideal capacitive performance in [EMIM][BF₄], outputting a high specific capacitance (270 F g^{-1}) and an ultrahigh energy density (133 Wh kg^{-1}). The facile aqueous phase synthesis as well as the impressive capacitive performance make the activated YSNCSs an ideal electrode material for high-performance EDLCs.

Results and Discussion

The preparation of micropore-rich YSNCSs is illustrated in Figure 1. First, core-shell structured organosilica@APF microspheres are synthesized via a one-pot sol-gel process, during which 3-aminophenol/formaldehyde (APF) is employed as the carbon source, vinyltrimethoxysilane (VTMS) is employed as the silicon source, and ammonia is used as the catalyst. The one-pot synthesis can avoid the labor- and time-consuming layer-by-layer coating, and the aqueous synthesis can avoid the employment of expensive organic solvent such as ethanol, making the scalable production more feasible.^[18] The yield of organosilica@APF can reach up to 27.61 g L^{-1} (Figure S1, Supporting Information). The activated YSNCSs are obtained after carbonization, HF etching, and subsequent KOH activation.

Microscopy characterizations show that both the organosilica@APF (Figure 2a–d) and the sample after carbonization (designated as SiO_x/C@C, Figure 2e–h) are comprised of uniform core-shell microspheres. To further confirm the distribution of organosilica and APF, the organosilica@APF was etched with HF before carbonization, which selectively etched the organosilica. Shrank hollow APF spheres (H-APF) with a cavity size of approximately 550 nm and a shell thickness of approximately

90 nm are obtained after HF etching (Figure S2a–d). In addition, the organosilica@APF was subjected to direct calcination in air, which burnt off the APF and organic moiety of organosilica but left silica (SiO₂). Rigid SiO₂ microspheres with a diameter of approximately 640 nm were obtained (Figure S2e–h). The above results unambiguously demonstrate the distribution of APF on organosilica in the organosilica@APF. Thermal gravimetric analysis (TGA) indicates the good thermostability of organosilica@APF with the decomposition starts from around 320 °C. Fourier-transform infrared spectroscopy (FTIR) uncovers abundant multifunctional groups of organosilica@APF, which primarily consists of amino groups and hydroxy groups. (Figure S3). High-angle annular dark field scanning transmission electron microscopy (HAADF-STEM) and energy-dispersive X-ray spectroscopy (EDS) elemental mappings (Figure 2i) show that C and N evenly distribute in the SiO_x/C@C particles, while O and Si mainly distribute in the internal SiO_x/C cores. With subsequent HF etching of the silicon oxide, monodisperse carbon microspheres with a well-defined yolk-shell structure (YSNCSs) are obtained (Figure 3a–d). The YSNCSs have an overall size of 570 nm, and the yolk size is approximately 350 nm while shell thickness is approximately 60 nm (Figure 3d, Figure S4a). The formation of yolk-shell structure is associated with the thermal treatment induced broken of Si–C bonds and shrinkage of the organosilica-derived carbon. When applied in EDLCs, it is expected that the void between the shell and yolk of YSNCSs can act as ion-buffering reservoirs to boost the performance.

To boost the surface area for capacitive storage, the YSNCS is subjected to KOH activation, and YSNCS-A is obtained after the activation. The KOH activation does not alter the overall morphology and structure of YSNCS significantly (Figure 3e–h) despite the slight shape change in the yolk. Compared with YSNCS, the central core size of YSNCS-A is reduced, and the cavity volume between the core and shell is enlarged. During the activation process, KOH etches part of the carbon away, leaving abundant micropores. This process inevitably breaks a small portion of the yolk-shell carbon spheres with such a high

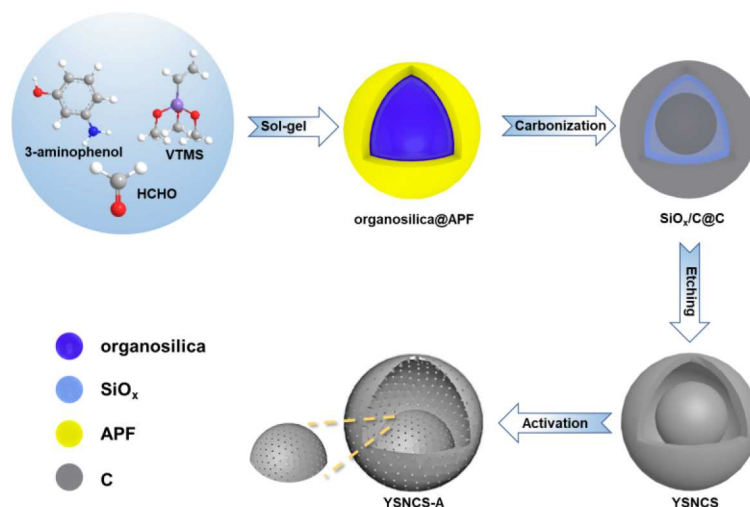


Figure 1. Schematic synthesis of YSNCS-A via sol-gel synthesis, carbonization, etching, and activation.

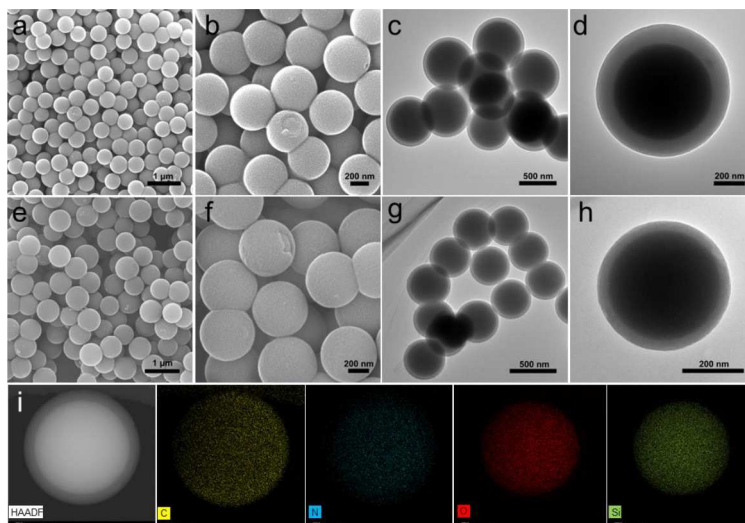


Figure 2. (a, b) SEM images and (c, d) TEM images of organosilica@APF. (e, f) SEM images and (g, h) TEM images of $\text{SiO}_x/\text{C}@\text{C}$. (i) HAADF-STEM image and the corresponding EDS elemental mappings of $\text{SiO}_x/\text{C}@\text{C}$.

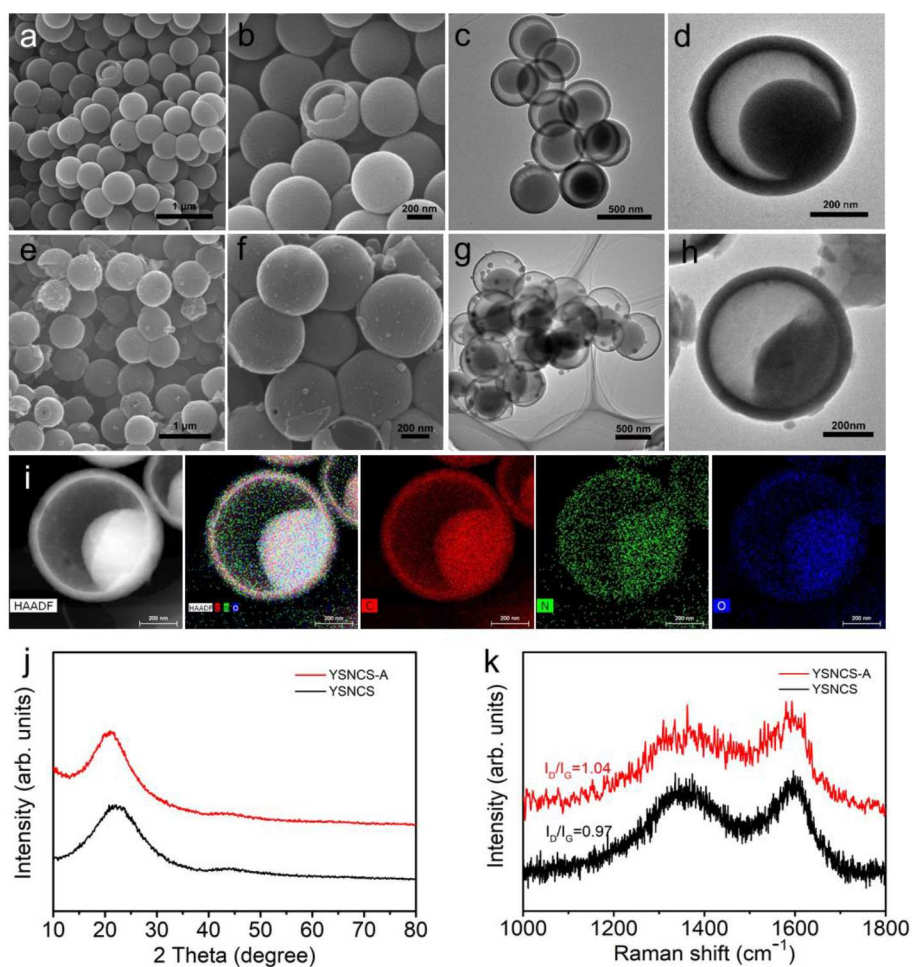


Figure 3. (a, b) SEM images and (c, d) TEM images of YSNCS. (e, f) SEM images and (g, h) TEM images of YSNCS-A. (i) HAADF-STEM image and the corresponding EDS elemental mappings of YSNCS-A. (j) XRD patterns of YSNCS-A and YSNCS. (k) Raman spectra of YSNCS-A and YSNCS.

KOH/YSNCS weight ratio (4:1). The YSNCS-A possesses a micropore-rich carbon shell of 50 nm (Figure 3h, Figure S4b), slightly thinner than that of YSNCS, demonstrating high corrosion resistance.^[19] The microporous shell is conducive to the infiltration of electrolyte, which can shorten the mass transfer distance. HAADF-STEM and EDS elemental mappings (Figure 3i) show that C, N, and O evenly distribute in the YSNCS-A particles. Selected area electron diffraction (SAED) pattern shows two halo-stained rings, demonstrating the amorphous state of YSNCS-A (Figure S4c). X-ray diffraction (XRD) patterns of YSNCS-A and YSNCS show two broad peaks at around 23 and 43.7°, corresponding to amorphous carbon (Figure 3j). The Raman spectra of both samples present a D-band at approximately 1340 cm⁻¹ and a G-band at 1590 cm⁻¹ with comparative intensities (Figure 3k), confirming their amorphous feature. The I_D/I_G ratio of YSNCS-A (1.04) is slightly higher than that of YSNCS (0.97) owing to the chemical activation, which introduces more defects.^[11a]

The surface area and pore size of YSNCS-A are studied by N₂ sorption. The YSNCS-A is micropore-rich, which can be reflected from the type I isotherm (Figure 4a) with sharp increase in adsorption amount at $P/P_0 < 0.1$. The abundant micropores afford the YSNCS-A a high surface area of 2536 m²g⁻¹. Such a surface area is three-fold over that of activated solid N-doped carbon spheres (NCS-A, 832 m²g⁻¹), and about 1.6 times to that of commercial YP-50F (1612 m²g⁻¹). Besides high surface area, the micropore-rich YSNCS-A also displays a large pore volume of 1.63 m³g⁻¹, which is over four times that of NCS-A (0.38 m³g⁻¹) and twice that of YP-50F (0.80 m³g⁻¹, Table S1).

The pore size distribution of YSNCS-A displays three peaks at 0.72, 1.30, and 2.75 nm (Figure 4b). The capacitive performance of porous carbons are highly dependent on their surface area and pore size.^[20] To make maximum utilization of the surface area, porous carbons with a pore size slightly larger than the size of electrolyte ions are required.^[4,20d] For [EMIM][BF₄], the [EMIM] cations and [BF₄] anions have sizes of 0.68 and 0.33 nm, respectively.^[21] Obviously, the pore size of YSNCS-A exceeds the size of [EMIM] cation and [BF₄] anion, suggesting the full accessibility of surface area to electrolyte ions. The electrolyte wettability of YSNCS-A towards [EMIM][BF₄] and water were studied by dynamic contact angle tests (Figure 4c). With [EMIM][BF₄], the initial contact angle is 60.0° and it reduces to 30.0° after 2 min. Conversely, the initial contact with water is 98.3° and it remains almost constant after 2 min. The dynamic contact angle tests demonstrate the excellent wettability of YSNCS-A towards [EMIM][BF₄].

The surface functionality of porous carbon contributes significantly to conductivity as well as electrolyte wettability.^[22] X-ray photoelectron spectroscopy (XPS) reveals the existence of C, N, and O in YSNCS and YSNCS-A. The C, N, and O atomic percentages are 90.97, 5.38, and 3.66% for YSNCS, and 95.61, 1.12, and 3.27% for YSNCS-A (Figure S5). The oxygen- and nitrogen-containing functional groups in the porous carbon materials may contribute to pseudocapacitance when applied in supercapacitors. However, they may decompose under high voltage window, leading to unsatisfactory cyclic stability. The secondary carbonization after KOH activation, which has also been adopted by supercapacitor industry, inevitably leads to decreased oxygen and nitrogen

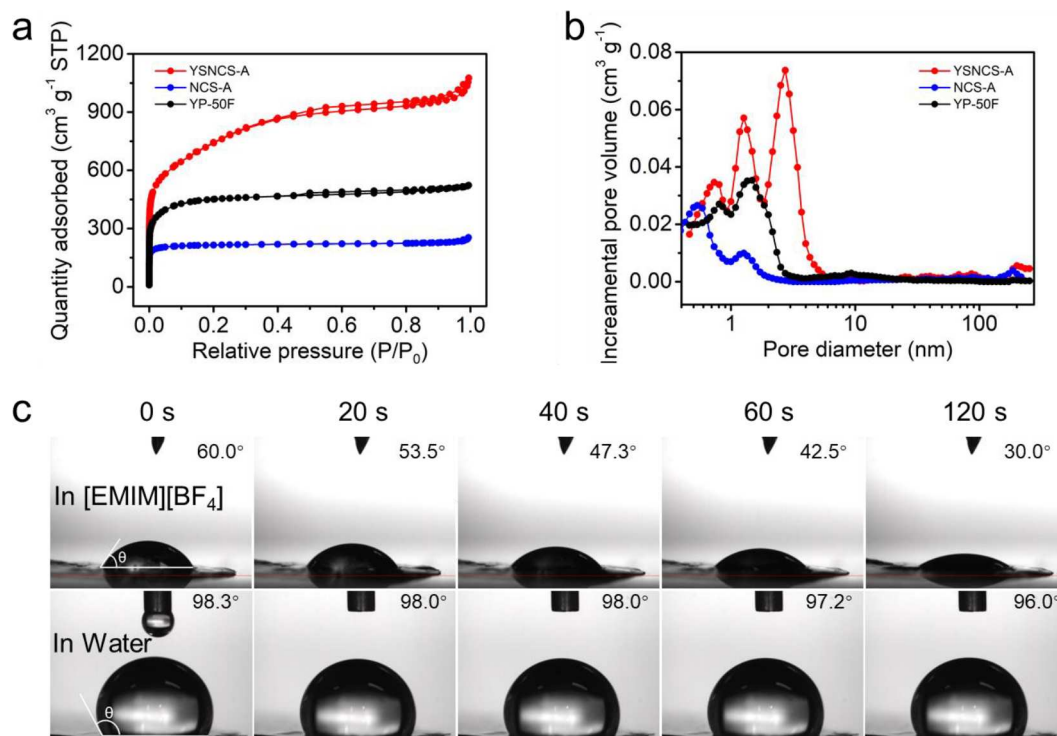


Figure 4. (a) N₂ adsorption/desorption isotherms of YSNCS-A, NCS-A, and YP-50F. (b) Corresponding pore size distributions of YSNCS-A, NCS-A, and YP-50F. (c) Dynamic contact angle measurement of YSNCS-A in [EMIM][BF₄] and water.

content but is beneficial for the cycling stability under high voltage window. The N1s core level spectrum can be fitted into three peaks at 398.4, 400.9, and 402.8 eV, corresponding to the pyridinic nitrogen (N-6), pyrrolic nitrogen (N-5), and graphitic nitrogen (N-Q), respectively (Figure S6).

To objectively evaluate the capacitive performance of YSNCS-A, commercial YP-50F, a benchmarking porous carbon material for EDLCs, is selected for comparison. To demonstrate that the enhanced capacitive performance of YSNCS-A benefits from not only the micropore-rich N-doped structure but also the yolk-shell structure, the activated solid N-doped carbon spheres (NCS-A) is selected for comparison as well. Two-electrode coin-cell supercapacitors are assembled with [EMIM][BF₄] as the electrolyte. The employment of [EMIM][BF₄] electrolyte enables a wide voltage window of 0–3.8 V. Cyclic voltammetry (CV) curves obtained at 100 mV s⁻¹ show typical EDLC behaviors: nearly symmetrical rectangular shapes for the YSNCS-A, NCS-A, and YP-50F (Figure 5a). The larger response current of YSNCS-A compared to NCS-A and YP-50F indicates its higher specific capacitance. The symmetric rectangular shape can still be maintained even at 1000 mV s⁻¹ (Figure 5b,c), manifesting the rapid kinetics.^[23] Galva-

nostatic charge/discharge (GCD) tests in a wide current density range of 1 to 50 A g⁻¹ show that YSNCS-A possesses significantly higher specific capacitance and rate performance than the NCS-A and YP-50F counterparts (Figure 5d,e and Figure S7). At 1 A g⁻¹, the capacitances for YSNCS-A, NCS-A, and YP-50F are 270, 158, and 198 F g⁻¹, respectively. The higher capacitance of YSNCS-A compared to NCS-A and YP-50F can be attributed to its higher specific surface area and more suitable pore size. Increasing the specific current to 50 A g⁻¹ leads to capacitance retentions of 76.6, 47.9, and 71.3% for YSNCS-A, NCS-A, and YP-50F, respectively. The carbonization temperature is a key parameter to obtain ideal carbon materials for EDLC applications. The carbonization temperature is varied from 700 to 900 °C. Among the three samples prepared at different carbonization temperatures, the sample prepared at 800 °C delivers the highest capacitance (270 F g⁻¹ at 1 A g⁻¹), while for the samples prepared at 700 and 900 °C, the capacitances are 184 and 240 F g⁻¹ (Figure S8), respectively. The capacitive performances of YSNCS-A are compared with other carbonaceous materials in IL electrolyte in the Ragone plots (Figure 5f) and Table S2.^[6a,10c,17a,24] Based on the active material mass, the YSNCS-A based supercapacitor demonstrates an ultra-

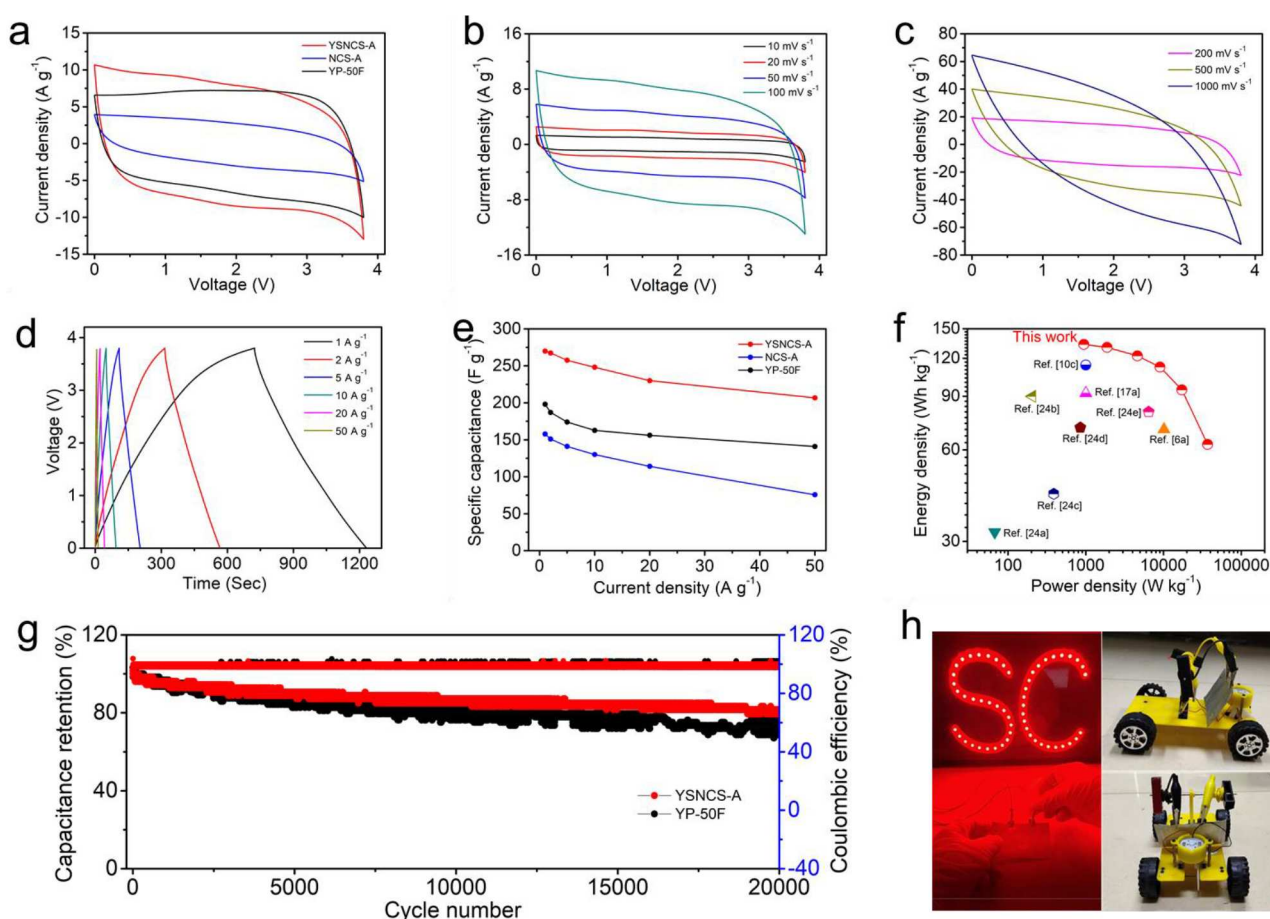


Figure 5. Electrochemical behaviors in [EMIM][BF₄] electrolyte: (a) CV profiles of YSNCS-A, NCS-A, and YP-50F at 100 mV s⁻¹. (b, c) CV profiles of YSNCS-A at various sweep rates. (d) GCD curves of YSNCS-A at various current densities. (e) Specific capacitances of YSNCS-A, NCS-A, and YP-50F as a function of GCD current density. (f) Comparison of the energy and power performances of YSNCS-A with other carbonaceous materials in IL electrolyte in the Ragone plots. (g) Stability test of YSNCS-A and YP-50F conducted at 5 A g⁻¹ for 20000 cycles in [EMIM][BF₄] ILs. (h) Digital photos demonstrating the potential of the assembled LEDs and toy car using YSNCS-A as electrode material in EDLCs.

high energy density of 133.33 Wh kg⁻¹ at 943 W kg⁻¹. Such a high value surpasses the energy density of most reported EDLCs. Assuming the porous carbon accounts for a quarter of the total mass of a real EDLC device, an energy density of 33 Wh kg⁻¹ is anticipated for the EDLC device.

Cycling stability is an important performance metric for EDLCs. The YSNCS-A based supercapacitor was cycled at 5 A g⁻¹ for 20000 cycles. The YSNCS-A demonstrates a capacitance retention of 88.2% after 10000 cycles and 80.0% after 20000 cycles with a coulombic efficiency of 99.4%, which surpasses the YP-50F (Figure S9). Electrical impedance spectroscopy (EIS) and the Nyquist plots with fitting curves confirm better capacitive behavior and rate performance of YSNCS-A than the NCS-A and YP-50F (Figure S9). Compared to NCS-A and YP-50F, the YSNCS-A has the smallest impedance semicircle at high frequency, which means that YSNCS-A possesses a lowest material intrinsic resistivity and highest electrical conductivity. The slope of YSNCS-A is closest to 90° at low-frequency region, indicating the highest ion diffusion rate. To understand the capacitance decay during cycling, GCD curves and EIS spectra of the YSNCS-A before and after cycling tests are provided (Figure S10). Obvious increase in internal resistance and decrease in ion diffusion can be noticed in the EIS spectrum after cycling (Figure S10b), which might be the reasons for the capacitance decay. To further evaluate the potential of YSNCS-A in EDLCs, a 5 cm × 3 cm supercapacitor device is assembled to light a "SC" circuit board composed of 52 light-emitting diodes (LEDs) in series and drive a 350 g toy car (Figure 5h). The assembled EDLC device is able to light up the circuit board for more than 20 min and drive a toy car for more than 60 m (Videos S1, S2).

Conclusions

Micropore-rich yolk-shell N-doped carbon spheres (YSNCS-A) were obtained through a surfactant-free self-assembly method in aqueous solution. With intriguing attributes of high surface area, rich micropores, appropriate pore size, ideal electrolyte wettability, and excellent conductivity, the YSNCS-A delivered a high specific capacitance of 270 F g⁻¹ at 1 A g⁻¹ and an outstanding rate performance of 207 F g⁻¹ at 50 A g⁻¹ in [EMIM][BF₄]. The high specific capacitance and wide electrochemical window of [EMIM][BF₄] worked together, affording an ultrahigh energy density of 133 Wh kg⁻¹ based on the mass of YSNCS-A.

Experimental Section

Chemicals: Formaldehyde, 3-aminophenol, ammonium hydroxide, vinyltrimethoxysilane (VTMS), [EMIM][BF₄], potassium hydroxide (KOH), and polytetrafluoroethylene (PTFE) were all purchased from Macklin Reagent Co. Among them, [EMIM][BF₄] was treated with molecular sieves for 24 h before use. The other chemicals used in the experiment were analytical grade and used without further purification.

Preparation of SiO_x/C@C: 3-Aminophenol (0.33 g) was first dissolved in deionized water (30 mL). Subsequently, VTMS (1 mL) and ammonia (1 mL) were added and stirred for 5 h at 25 °C.

Formaldehyde (456 μL) was added dropwise and stirred for another 5 h. After the reaction, the precipitates were collected by centrifugation, washed, and then dried. The as-synthesized sample (organosilica@APF) was carbonized at 800 °C for 3 h in Ar to obtain the SiO_x/C@C.

Preparation of YSNCS-A: The as-prepared SiO_x/C@C was treated with 10% HF solution to obtain the YSNCS by removing the silicon oxide. The YSNCSs were activated with a KOH/YSNCS mass ratio of 4:1 at 700 °C for 1 h in flowing Ar and the heating rate was 2 °C min⁻¹. The obtained mixture was washed with diluted HCl and deionized water to neutral and dried overnight to get the final product YSNCS-A.

Preparation of NCS-A: 3-Aminophenol (0.33 g) was dissolved in deionized water (30 mL). Subsequently, formaldehyde (456 μL) was added dropwise and stirred for 30 min. The precipitates were collected by centrifugation, washed, and then dried. The as-synthesized sample (APF) was then carbonized and activated to obtain NCS-A.

Fabrication of coin-cell supercapacitors: The electrochemical performances were evaluated in [EMIM][BF₄] with a two-electrode configuration. First, the electrode was prepared by grinding the active material, acetylene black, PTFE with a mass ratio of 8:1:1 until a shiny chewing gum type black mud was produced. The mud was rolled into sheets and punched into small discs with diameter of 8 mm, which was then dried at 70 °C for 48 h. Then, the carbon electrode was loaded onto a nickel foam, pressurized to 10 MPa and maintained for 30 s. Two electrodes and 2025-type coin cell were assembled into a symmetrical two-electrode cell in an Ar-filled glovebox (with O₂ and H₂O contents below 1 ppm) with [EMIM][BF₄] and cellulose as electrolyte and separator, respectively.

Materials characterization: SEM images were obtained on a JEOL-7100F scanning electron microscope at 20 kV. TEM images and EDS elemental mappings were collected on a JEM-2100F microscope at 200 kV. XRD patterns were obtained on a D8 Advance X-ray diffractometer with a Cu K_α X-ray source. Raman spectra were collected on a confocal micro-Raman system (WITec alpha 300) using a diode laser (excitation wavelength: 532 nm). The Brunauer–Emmett–Teller (BET) surface areas and pore volumes were calculated from N₂ sorption results on an ASAP-2020 instrument at 77 K. Dynamic contact angle measurements were obtained on a SZ10-JC2000 C instrument. XPS results were obtained using a ESCALAB 250Xi instrument. FTIR spectroscopy was performed on KBr pellets using a Perkin–Elmer spectrum IR Affinity-1 spectrometer. TGA was conducted using a STA-449C thermogravimetric apparatus.

Measurements of electrochemical performance: The electrochemical performances were characterized by CV, GCD, and EIS on a CHI 760E electrochemical workstation (Chenhua Instruments, China) and the cyclic stability was characterized on NEWARE testing system. The gravimetric specific capacitance of the single electrode C_s [F g⁻¹] was obtained by Equation (1):

$$C_s = 4 \times \frac{I \Delta t}{m_t \Delta U} \quad (1)$$

where *I* is the current, Δt is the discharge time, ΔU is the potential range (excluding the voltage drop), and *m_t* is the total mass of the YSNCS-A on both electrodes.

Note: For symmetrical EDLCs, the single electrode and the cell have the same amount of charge, while the voltage and mass of the cell are twice that of the single electrode. Consequently, the capacitance of the cell C_c is converted to the specific capacitance of the single electrode material with the factor 4. That is C_c = 1/4 C_s.

The energy density of the cell E [Wh kg⁻¹] is calculated from the following Equation (2):

$$E = \frac{C_s (\Delta U)^2}{2 \times 4 \times 3.6} \quad (2)$$

3.6 is the unit conversion from Jg⁻¹ to Wh kg⁻¹.

The power density of the cell P [W kg⁻¹] is calculated based on Equation (3):

$$P = \frac{3600 \times E}{\Delta t} \quad (3)$$

Acknowledgements

This work was supported by the National Natural Science Foundation of China (52072283), the State Key Laboratory of Advanced Technology for Materials Synthesis and Processing (WUT: 2020-KF-3), the Fundamental Research Funds for the Central Universities (WUT: 2020-zy-020), Foshan Xianhu Laboratory of the Advanced Energy Science and Technology Guangdong Laboratory (XHT2020-003).

Conflict of Interest

The authors declare no conflict of interest.

Keywords: Capacitors · carbon spheres · energy density · micropores · yolk-shell structure

- [1] a) H. Shao, Y. Wu, Z. Lin, P.-L. Taberna, P. Simon, *Chem. Soc. Rev.* **2020**, *49*, 3005; b) Y. Zhai, Y. Dou, D. Zhao, P. F. Fulvio, R. T. Mayes, S. Dai, *Adv. Mater.* **2011**, *23*, 4828; c) P. Simon, Y. Gogotsi, *Acc. Chem. Res.* **2013**, *46*, 1094.
- [2] P. Simon, Y. Gogotsi, B. Dunn, *Science* **2014**, *343*, 1211.
- [3] a) T. Wang, F. Okejiri, Z. A. Qiao, S. Dai, *Adv. Mater.* **2020**, *32*, 2002475; b) G. Wang, Y. Sun, D. Li, H. Liang, R. Dong, X. Feng, K. Müllen, *Angew. Chem. Int. Ed.* **2015**, *54*, 15191; *Angew. Chem.* **2015**, *127*, 15406.
- [4] a) J. Chmiola, G. Yushin, Y. Gogotsi, C. Portet, P. Simon, P. L. Taberna, *Science* **2006**, *313*, 1761; b) C. Largeot, C. Portet, J. Chmiola, P.-L. Taberna, Y. Gogotsi, P. Simon, *J. Am. Chem. Soc.* **2008**, *130*, 2730.
- [5] a) T. Lin, I.-W. Chen, F. Liu, C. Yang, H. Bi, F. Xu, F. Huang, *Science* **2015**, *350*, 1509; b) G. Shen, X. Sun, H. Zhang, Y. Liu, J. Zhang, A. Meka, L. Zhou, C. Yu, *J. Mater. Chem. A* **2015**, *3*, 24041.
- [6] a) Y. Zhu, S. Murali, M. D. Stoller, K. J. Ganesh, W. Cai, P. J. Ferreira, A. Pirkle, R. M. Wallace, K. A. Cychosz, M. Thommes, D. Su, E. A. Stach, R. S. Ruoff, *Science* **2011**, *332*, 1537; b) X. Yang, C. Cheng, Y. Wang, L. Qiu, D. Li, *Science* **2013**, *341*, 535; c) Z. Li, S. Gadipelli, H. Li, C. A. Howard, D. J. L. Brett, P. R. Shearing, Z. Guo, I. P. Parkin, F. Li, *Nat. Energy* **2020**, *5*, 160.
- [7] Q. Hu, Z. Lu, Y. Wang, J. Wang, H. Wang, Z. Wu, G. Lu, H. Zhang, C. Yu, *J. Mater. Chem. A* **2020**, *8*, 13095.
- [8] a) Q. Yu, J. Lv, Z. Liu, M. Xu, W. Yang, K. A. Owusu, L. Mai, D. Zhao, L. Zhou, *Sci. Bull.* **2019**, *64*, 1617; b) L. Chen, Y. Lu, L. Yu, X. W. Lou, *Energy Environ. Sci.* **2017**, *10*, 1777.
- [9] a) Z. Jin, A. Lu, Y. Xu, J. Zhang, W. Li, *Adv. Mater.* **2014**, *26*, 3700; b) X. Zheng, W. Lv, Y. Tao, J. Shao, C. Zhang, D. Liu, J. Luo, D. Wang, Q. Yang, *Chem. Mater.* **2014**, *26*, 6896; c) Z. Xiong, C. Liao, W. Han, X. Wang, *Adv. Mater.* **2015**, *27*, 4469; d) H. Huang, R. Xu, Y. Feng, S. Zeng, Y. Jiang, H. Wang, W. Luo, Y. Yu, *Adv. Mater.* **2020**, *32*, 1904320.
- [10] a) J. Zhao, H. Lai, Z. Lyu, Y. Jiang, K. Xie, X. Wang, Q. Wu, L. Yang, Z. Jin, Y. Ma, J. Liu, Z. Hu, *Adv. Mater.* **2015**, *27*, 3541; b) Q. Wu, L. Yang, X. Wang, Z. Hu, *Acc. Chem. Res.* **2017**, *50*, 435; c) Y. Bu, T. Sun, Y. Cai, L. Du, O. Zhuo, L. Yang, Q. Wu, X. Wang, Z. Hu, *Adv. Mater.* **2017**, *29*, 1700470.
- [11] a) M. Xu, Q. Yu, Z. Liu, J. Lv, S. Lian, B. Hu, L. Mai, L. Zhou, *Nanoscale* **2018**, *10*, 21604; b) S. Feng, Z. Liu, Q. Yu, Z. Zhuang, Q. Chen, S. Fu, L. Zhou, L. Mai, *ACS Appl. Mater. Interfaces* **2019**, *11*, 4011; c) T. Wang, Y. Sun, L. Zhang, K. Li, Y. Yi, S. Song, M. Li, Z. Qiao, S. Dai, *Adv. Mater.* **2019**, *31*, 1807876.
- [12] H. Luo, Z. Liu, L. Chao, X. Wu, X. Lei, Z. Chang, X. Sun, *J. Mater. Chem. A* **2015**, *3*, 3667.
- [13] a) J. Wang, S. Feng, Y. Song, W. Li, W. Gao, A. A. Elzatory, D. Aldhayan, Y. Xia, D. Zhao, *Catal. Today* **2015**, *243*, 199; b) F. Pei, L. Lin, D. Ou, Z. Zheng, S. Mo, X. Fang, N. Zheng, *Nat. Commun.* **2017**, *8*, 482.
- [14] Z. Qiao, B. Guo, A. J. Binder, J. Chen, G. M. Veith, S. Dai, *Nano Lett.* **2012**, *13*, 207.
- [15] a) C. Liu, J. Wang, J. Li, R. Luo, J. Shen, X. Sun, W. Han, L. Wang, *ACS Appl. Mater. Interfaces* **2015**, *7*, 18609; b) C. Liu, J. Wang, J. Li, M. Zeng, R. Luo, L. Shen, X. Sun, W. Han, L. Wang, *ACS Appl. Mater. Interfaces* **2016**, *8*, 7194; c) C. Liu, J. Wang, J. Li, X. Hu, P. Lin, J. Shen, X. Sun, W. Han, L. Wang, *J. Mater. Chem. A* **2016**, *4*, 11916.
- [16] Z. Liu, H. Song, Y. Zhao, R. He, J. Meng, Q. Yu, K. A. Owusu, C. Yu, D. Zhao, L. Zhou, L. Mai, *ACS Materials Lett.* **2019**, *1*, 290.
- [17] a) J. Li, N. Wang, J. Tian, W. Qian, W. Chu, *Adv. Funct. Mater.* **2018**, *28*, 1806153; b) R. Gao, J. Tang, X. Yu, S. Lin, K. Zhang, L. Qin, *Adv. Funct. Mater.* **2020**, *30*, 2002200; c) Y. Wang, B. Li, S. Sarman, F. Mocci, Z. Lu, J. Yuan, A. Laaksonen, M. D. Fayer, *Chem. Rev.* **2020**, *120*, 5798; d) M. Shi, S. Kou, X. Yan, *ChemSusChem* **2014**, *7*, 3053; e) L. Ma, Q. Gao, W. Tian, Q. Zhang, H. Xiao, Z. Li, H. Zhang, X. Tian, *ChemSusChem* **2018**, *11*, 4026.
- [18] A. B. Fuertes, P. Valle-Vigón, M. Sevilla, *Chem. Commun.* **2012**, *48*, 6124.
- [19] a) J. Liu, S. Qiao, H. Liu, J. Chen, A. Orpe, D. Zhao, G. Lu, *Angew. Chem. Int. Ed.* **2011**, *50*, 5947; *Angew. Chem.* **2011**, *123*, 6069; b) P. Zhang, Z. Qiao, S. Dai, *Chem. Commun.* **2015**, *51*, 9246; c) J. Liu, N. P. Wickramaratne, S. Qiao, M. Jaroniec, *Nat. Mater.* **2015**, *14*, 763.
- [20] a) H. Peng, B. Yao, X. Wei, T. Liu, T. Kou, P. Xiao, Y. Zhang, Y. Li, *Adv. Energy Mater.* **2019**, *9*, 1803665; b) Y. Chi, C. Hu, H. Shen, K. Huang, *Nano Lett.* **2016**, *16*, 5719; c) F. Wu, H. Lv, S. Chen, S. Lörger, V. Srot, M. Oschatz, P. Aken, X. Wu, J. Maier, Y. Yu, *Adv. Funct. Mater.* **2020**, *29*, 1902820; d) R. Levie, *Electrochim. Acta* **1963**, *8*, 751.
- [21] a) E. H. Lahrar, A. Belhboub, P. Simon, C. Merlet, *ACS Appl. Mater. Interfaces* **2019**, *12*, 1789; b) C. Péan, C. Merlet, B. Rotenberg, P. A. Madden, P.-L. Taberna, B. Daffos, M. Salanne, P. Simon, *ACS Nano* **2014**, *8*, 1576; c) C. R. Pérez, S.-H. Yeon, J. Ségalini, V. Presser, P.-L. Taberna, P. Simon, Y. Gogotsi, *Adv. Funct. Mater.* **2013**, *23*, 1081.
- [22] a) M. Zhang, L. He, T. Shi, R. Zha, *Chem. Mater.* **2018**, *30*, 7391; b) G. Hasegawa, T. Deguchi, K. Kanamori, Y. Kobayashi, H. Kageyama, T. Abe, K. Nakanishi, *Chem. Mater.* **2015**, *27*, 4703; c) Z. Song, D. Zhu, L. Li, T. Chen, H. Duan, Z. Wang, Y. Lv, W. Xiong, M. Liu, L. Gan, *J. Mater. Chem. A* **2019**, *7*, 1177.
- [23] a) J. Segalini, E. Iwama, P.-L. Taberna, Y. Gogotsi, P. Simon, *Electrochem. Commun.* **2012**, *15*, 63; b) J. M. Griffin, A. C. Forse, W.-Y. Tsai, P.-L. Taberna, P. Simon, C. P. Grey, *Nat. Mater.* **2015**, *14*, 812.
- [24] a) H. Wang, S. Yu, B. Xu, *Chem. Commun.* **2016**, *52*, 11512; b) Z. Song, H. Duan, L. Li, D. Zhu, T. Cao, Y. Lv, W. Xiong, Z. Wang, M. Liu, L. Gan, *Chem. Eng. J.* **2019**, *372*, 1216; c) Y. Lian, M. Ni, Z. Huang, R. Chen, L. Zhou, W. Utetiwo, W. Yang, *Chem. Eng. J.* **2019**, *366*, 313; d) X. Yang, C. Cheng, Y. Wang, L. Qiu, D. Li, *Science* **2013**, *341*, 535; e) Y. Xu, Z. Lin, X. Zhong, X. Huang, N. O. Weiss, Y. Huang, X. Duan, *Nat. Commun.* **2014**, *5*, 4554.

Manuscript received: January 15, 2021

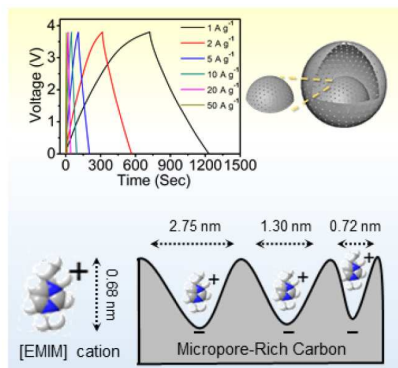
Revised manuscript received: February 1, 2021

Accepted manuscript online: February 3, 2021

Version of record online: ■■■, ■■■■

FULL PAPERS

Super spheres: Micropore-rich yolk-shell structured N-doped carbon spheres (YSNCSs) are constructed by a one-pot surfactant-free self-assembly method. The resultant YSNCSs after activation demonstrate an unprecedentedly high specific capacitance of 270 F g^{-1} at 1 A g^{-1} and an excellent rate performance of 207 F g^{-1} at 50 A g^{-1} in [EMIM][BF₄], affording an ultrahigh energy density of 133 Wh kg^{-1} .



X. Li, Dr. Z. Liu, C. Cai, Dr. Q. Yu, W. Jin, M. Xu, C. Yu, S. Li, Prof. L. Zhou, Prof. L. Mai**

1 – 8

Micropore-Rich Yolk-Shell N-doped Carbon Spheres: An Ideal Electrode Material for High-Energy Capacitive Energy Storage

